Showcasing research from the laboratory of Dr Kazuhide Kamiya at the Graduate School of Engineering Science, The University of Osaka, Japan.

Alkali-cation-free electrochemical CO_2 reduction to multicarbon products in aqueous electrolytes containing tetraalkylammonium cations

Alkali-cation-free CO_2 electrolysis is important to address the issue of salt precipitation. We investigated the effect of tetraalkylammonium cations on C_{2+} formation. With tetramethylammonium, the C_{2+} selectivity on Cu reached 69.6% at 1 A cm^{-2}. Theoretical simulations show that smaller cations intensify the electric fields within the electric double layer that stabilize the reaction intermediates, boosting C_{2+} formation. These findings offer valuable insights into the design of alkali-cation-free, pure-water-fed membrane electrode assembly electrolysis.

Image reproduced by permission of Kazuhide Kamiya from *EES Catal.*, 2025, **3**, 1055.

As featured in:

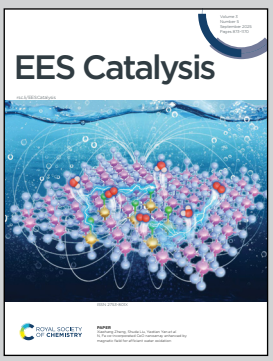

See Kazuhide Kamiya *et al.*, *EES Catal.*, 2025, **3**, 1055.

ROYAL SOCIETY OF CHEMISTRY

rsc.li/EESCatalysis

Registered charity number: 207890

EES Catalysis

PAPER

View Article Online
View Journal | View Issue

Cite this: *EES Catal.*, 2025, 3, 1055

Alkali-cation-free electrochemical CO_2 reduction to multicarbon products in aqueous electrolytes containing tetraalkylammonium cations†

Ryo Kurihara,[a] Shotaro Ito,[a] Shintaro Kato,[a] Takashi Harada,[ab] Shuji Nakanishi[ab] and Kazuhide Kamiya*[ab]

Received 12th May 2025,
Accepted 29th June 2025

DOI: 10.1039/d5ey00141b

rsc.li/eescatalysis

The electrochemical reduction of CO_2 to multicarbon (C_{2+}) products is attracting attention for the sustainable production of fuel and chemicals. Conventionally, electrolytes containing alkali cations are typically used; however, salt precipitation associated with these cations often hinders stable CO_2 electrolysis. Organic cations are promising alternatives to alkali cations. Herein, we conducted gaseous CO_2 electrolysis in aqueous solutions containing tetraalkylammonium cations in the absence of alkali cations to evaluate the effect of organic cations on C_{2+} formation. When tetramethylammonium cations were present as the only cation species besides protons, the faradaic efficiency for CO_2 reduction exceeded 89% across a broad current density range of 0.1–1 A cm^{-2}. In particular, C_{2+} formation was efficient under high total current density conditions, reaching a faradaic efficiency of 69.6% and a partial current density of 0.7 A cm^{-2}. By contrast, the use of larger cations such as tetraethylammonium and tetrapropylammonium cations resulted in lower ethylene selectivity. Numerical simulations based on the generalized modified Poisson–Nernst–Planck model suggested that the size of the tetraalkylammonium cations affects the electric field strength within the electric double layer, with smaller cations forming a stronger field that promotes ethylene formation.

Broader context

Electrochemical CO_2 reduction offers a direct route to closing the carbon loop using renewable electricity. The production of multicarbon (C_{2+}) products using Cu catalysts is particularly attractive; however, conventional systems depend on alkaline electrolytes such as $KHCO_3$ or KOH. Alkali cations tend to precipitate as carbonate salts within porous gas diffusion electrodes, compromising long-term stability. As a result, alkali-cation-free electrolysis is gaining increasing attention. One promising strategy involves replacing alkali cations with organic cations bearing a tetraalkylammonium moiety. Here, we performed gaseous CO_2 electrolysis in aqueous solutions containing tetraalkylammonium cations, without any alkali cations, to investigate the influence of these organic cations on C_{2+} product formation. When tetramethylammonium was the sole cation species present apart from protons, industrially relevant current densities for C_{2+} production were achieved. In contrast, the use of bulkier cations such as tetraethylammonium and tetrapropylammonium led to decreased C_{2+} selectivity. These findings offer valuable insights into the design of alkali-cation-free, pure-water-fed membrane electrode assembly electrolyzers where organic cations, including cationic ionomers, serve as the primary electrolyte species.

1. Introduction

The efficient reduction and conversion of CO_2, a greenhouse gas contributing to global warming, is crucial for achieving a carbon-neutral society.[1–3] The electrochemical CO_2 reduction reaction (CO_2RR) in aqueous systems has attracted attention as a CO_2 conversion process that operates under ambient conditions.[4–6] In particular, the selective production of high-value C_{2+} products by Cu catalysts, such as ethylene, ethanol, and acetate, is highly desirable for their use as sustainable fuels and as renewable feedstocks for carbon-based fine chemicals.[7–14] The operational efficiency, selectivity, and formation rate for C_{2+} products are critical factors determining the feasibility of device implementation.

The selectivity and kinetics of the CO_2RR are influenced by multiple factors, including electrocatalysts, electrodes, and

[a] *Research Center for Solar Energy Chemistry, Graduate School of Engineering Science, The University of Osaka, 1-3 Machikaneyama, Toyonaka, Osaka 560-8531, Japan. E-mail: kamiya.kazuhide.es@osaka-u.ac.jp*

[b] *Innovative Catalysis Science Division, Institute for Open and Transdisciplinary Research Initiatives (ICS-OTRI), The University of Osaka, 1-1 Yamadaoka, Suita, Osaka 565-0871, Japan*

† Electronic supplementary information (ESI) available. See DOI: https://doi.org/10.1039/d5ey00141b

electrolyzers.[15–18] Electrolytes also play a critical role in determining CO_2RR activity. For instance, alkali cations, such as K^+ and Cs^+, are known to enhance CO and C_{2+} formation by coordinating with reaction intermediates[19–22] and generating stronger electric fields within the electric double layer (EDL).[23–27] However, the use of alkali-cation-containing electrolytes leads to (bi)carbonate salt precipitation, which compromises system stability.[13,28–31] Conducting CO_2 electrolysis in the absence of alkali cations is expected to substantially improve the long-term stability of the system.

Organic cations have been proposed as potential alternatives to alkali cations. Recent studies have demonstrated the CO_2RR under alkali-cation-free conditions using organic cations as electrolytes. Weng *et al.* reported CO formation on Au and Ag electrodes using tetraethylammonium and poly(dimethyl diallyl ammonium) cations in the absence of alkali cations.[32] Similarly, Jang *et al.* observed CO production on a Au electrode with cetyltrimethylammonium cations under alkali-cation-free conditions.[33] Regarding C_{2+} production on Cu catalysts, organic cations have been explored primarily as ionomers or surfactants on electrode surfaces.[34–38] However, most studies on C_{2+} production involving organic cations have been conducted under conditions where alkali cations are also present. Gao *et al.* conducted CO_2RR on Cu catalysts using an electrolyte that contained only piperidinium cations and reported that the aggregation state of piperidinium cations affects CO_2RR activity.[39] Although their study is regarded as pioneering for utilizing solely organic cations in the system, no study has yet examined CO_2RR on Cu catalysts in which the simplest and most representative tetraalkylammonium cation serves as the sole cation species in aqueous solution. Therefore, the effects of organic-cation structure and size on CO_2RR on Cu catalysts remain poorly understood. Furthermore, the impact of organic cations on gas-fed CO_2 electrolysis in flow cells has not been investigated under practically relevant high current density conditions. The lack of studies on such C_{2+} production reactions is likely attributable to the complexity of the CO_2RR on Cu catalysts, which involves multi-electron transfer beyond two electrons, resulting in diverse products and complex reaction mechanisms. Thus, how organic cations affect C_{2+} formation and the C_{2+} formation mechanism, and which specific cations facilitate C_{2+} production remain unclear. A comprehensive understanding of organic cation effects is essential for advancing the CO_2RR in pure-water-fed membrane electrode assembly (MEA) systems, where alkali cations are absent and cationic ionomers are expected to function as the primary electrolyte cations.[38,40–42]

In the present study, we investigated the CO_2RR to produce C_{2+} products in alkaline aqueous solutions containing tetraalkylammonium cations with various alkyl chain lengths under industry-relevant current densities (>100 mA cm^{-2}). Tetraalkylammonium cations are commonly used as side chains in anion-exchange ionomers, and their size can be readily tuned by modifying the alkyl chain length. This is the first study to demonstrate C_{2+} production in an aqueous electrolyte with tetraalkylammonium cations. Our findings reveal that smaller cations lead to higher ethylene production rates. When TMA was used, the faradaic efficiency for C_{2+} reached a maximum of 69.6% at a total current density of 1000 mA cm^{-2}. In addition, to elucidate the role of tetraalkylammonium cations at the electrode–electrolyte interface, we conducted numerical simulations to analyze cation effects within the EDL.

2. Results and discussion

We pasted 100 nm-diameter CuO nanoparticles (CuONPs) onto gas diffusion electrodes (GDEs). Details of the characterization of our catalyst and electrode are shown in the Supporting Information. Briefly, X-ray photoelectron spectroscopy (XPS) and X-ray absorption near edge structure (XANES) spectra (Fig. S1 and S2, respectively, ESI†) show that the oxidation state of Cu both on the surface and in the bulk was Cu(II). The X-ray diffraction (XRD) pattern shows peaks at 35.5° and 38.7°, which correspond to the CuO(002) and CuO(111) planes (Fig. S3, ESI†). Fig. S4 (ESI†) shows a scanning electron microscopy (SEM) image of the CuONPs. Fig. S5 (ESI†) shows a cross-sectional SEM image and corresponding energy-dispersive X-ray (EDX) mapping image of the CuONPs/GDE. The thickness

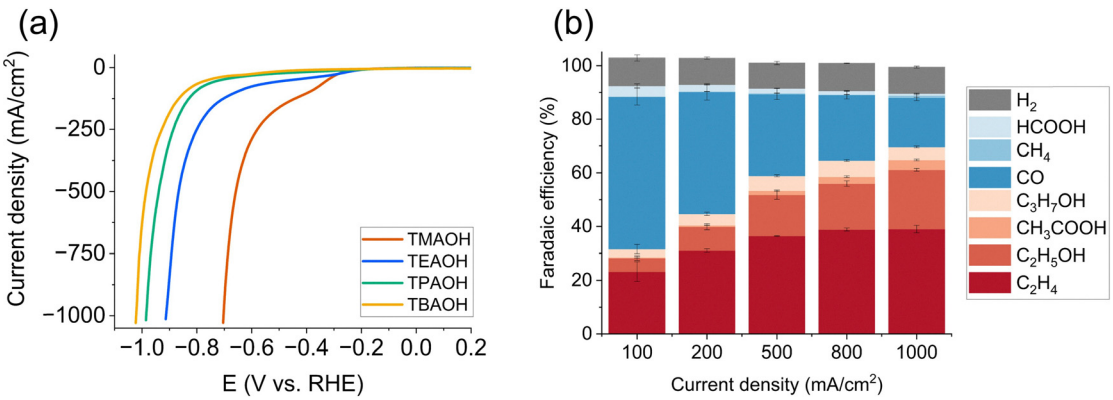

Fig. 1 (a) Linear-sweep voltammograms recorded in different tetraalkylammonium hydroxide solutions (1.0 M) under CO_2 gas. (b) Faradaic efficiency of CO_2RR in 1.0 M tetramethylammonium hydroxide solutions at different current densities.

of the CuONPs catalyst layer was approximately 1–2 μm. The surface of the microporous layer was almost fully covered by CuONPs.

We investigated the CO_2 reduction behavior in tetraalkylammonium hydroxide aqueous solutions using a custom-made three-compartment cell (Fig. S6, ESI†). Fig. 1(a) and Fig. S7 (ESI†) show the current density *vs.* potential curves for our electrode in 1.0 M tetramethylammonium hydroxide (TMAOH), tetraethylammonium hydroxide (TEAOH), tetrapropylammonium hydroxide (TPAOH), and tetrabutylammonium hydroxide (TBAOH) under continuous CO_2 or Ar delivery conditions. The applied potential was compensated for using the current interruption method[43,44] (see ESI† for details). Under CO_2 supply conditions, a high cathodic current density (>100 mA cm^{-2} at -0.40 V *vs.* reversible hydrogen electrode (RHE)) was obtained in TMAOH, whereas the current density was less than 100 mA cm^{-2} at -0.40 V *vs.* RHE in TEAOH, TPAOH, and TBAOH. In the TPAOH and TBAOH electrolytes, the current density under Ar conditions was greater than that under CO_2 conditions (Fig. S8, ESI†).

We next analyzed the products of the CO_2RR carried out under galvanostatic conditions. The faradaic efficiencies (FEs) of CO_2RR products in 1.0 M TMAOH solutions are shown in Fig. 1(b). At all examined current densities, the FE for H_2 production was approximately 10% and the major products were CO, C_2H_4, and C_2H_5OH. Although CO was the major product (FE for CO = 57%) at 100 mA cm^{-2}, the C_{2+} selectivity increased with increasing current density. At a total current density of 1000 mA cm^{-2}, the FEs for C_2H_4, C_2H_5OH, acetic acid, and *n*-propanol reached 39.0%, 22.1%, 3.7%, and 4.8%, respectively, resulting in an overall C_{2+} selectivity of 69.6% with a corresponding partial current density of 696 mA cm^{-2}. The present study represents the first report on CO_2 electrolysis in an aqueous solution containing tetraalkylammonium cations, and the maximum C_{2+} partial current density achieved here represents the highest reported production rate for CO_2 electrolysis using organic cations, including ionomer-based systems.[38,41,42,45] When the current density exceeded 1500 mA cm^{-2}, the catalyst layer became flooded with electrolytes, leading to the cessation of electrolysis. The tendency for the FE for C_{2+} to increase with increasing current density while the production of CO decreases monotonically is a common phenomenon when alkali cation solutions are used. The CO partial pressure in the catalyst layer increases with increasing current density, implying a corresponding decrease in the CO_2 partial pressure. Consequently, the reduction of CO to C_{2+} is favored over the reduction of CO_2 to CO, which leads to an increase in the FE for C_{2+} products.[13] CO_2RR stability was evaluated in a 1.0 M TMAOH solution, showing sustained ethylene selectivity for over 10 hours (Fig. S9, ESI†). It should be noted that the duration over which C_{2+} production activity is maintained can vary significantly depending on the electrolyzer configuration and electrode materials.

To examine the influence of cation size on product selectivity, we evaluated the CO_2RR activity in TEAOH and TPAOH solutions and compared the results with those for a TMAOH solution. As shown in Fig. S10(a) and (b) (ESI†), the major gaseous product of the CO_2RR was CO in both the TEAOH and TPAOH solutions. The FE for C_2H_4 slightly increased with increasing current density, reaching a maximum value of 14.7% in TEAOH at 500 mA cm^{-2} and 7.1% in TPAOH at 300 mA cm^{-2}. These values are substantially lower than the maximum value of 39.0% in TMAOH at 1000 mA cm^{-2}. By contrast, the FE for CO monotonically decreased with increasing current density across all three solutions. At higher current densities, H_2 and methane production apparently increased in the TEAOH and TPAOH solutions. With larger cationic species, the FE for H_2 and CH_4 started to increase at lower current densities.

We conducted inductively coupled plasma optical emission spectroscopy (ICP-OES) measurements to quantitatively determine the concentration of alkali cation contaminants in TMAOH electrolyte. The CO_2RR was conducted at 500 mA cm^{-2} in 1.0 M TMAOH (Fig. S11, ESI†), and Li, Na, and K in the cathode electrolyte were quantified before and after electrolysis. Table S1 (ESI†) shows the concentration of Li, Na, and K in the tested solutions. The concentrations of Na and K in the pre- and post-electrolysis TMAOH samples showed no significant increase compared to the acid blank (approximately 0.20 mM; see the note in Table S1 for details, ESI†), and were therefore considered below the limit of quantification. Furthermore, to rule out the possibility that trace alkali cations affect C_{2+} formation, we intentionally introduced 0.10–0.50 mM NaOH into a 1.0 M TPAOH electrolyte and carried out CO_2RR (Fig. S12, ESI†). Compared with the Na-free control experiment, no significant difference was observed in the faradaic efficiency for ethylene. These observations indicate that even if trace alkali cations at concentrations on the order of 0.50 mM are present, their influence on C_{2+} formation is limited. Considering the ICP-OES results and the alkali cation addition experiments, the influence of contaminant alkali cations on C_{2+} formation is considered negligible.

To more closely examine how the cation in the electrolyte affects the CO_2RR products, we investigated the potential dependence of product formation. Fig. 2 shows plots of the partial current density for each gaseous product against the applied potential. The partial current density for CO and ethylene increased at more positive potentials when smaller cations were used (Fig. 2(a) and (b)). Specifically, TMA triggered ethylene production starting at -0.4 V *vs.* RHE, reaching 390 mA cm^{-2} at maximum. By comparison, TEA and TPA required more negative potentials to initiate ethylene formation, reaching maximum partial current densities of 93.4 mA cm^{-2} and 24.6 mA cm^{-2}, respectively. In contrast, the partial current density for methane drastically increased at potentials more negative than -0.85 V *vs.* RHE when TEA or TPA was used, reaching 144 mA cm^{-2} and 102 mA cm^{-2} at maximum, respectively (Fig. 2(c)). With TMA, the most negative potential tested was approximately -0.7 V *vs.* RHE, and no substantial increase in methane production was observed. Hence, the formation rates of ethylene and CO improved substantially when smaller cations were used, whereas

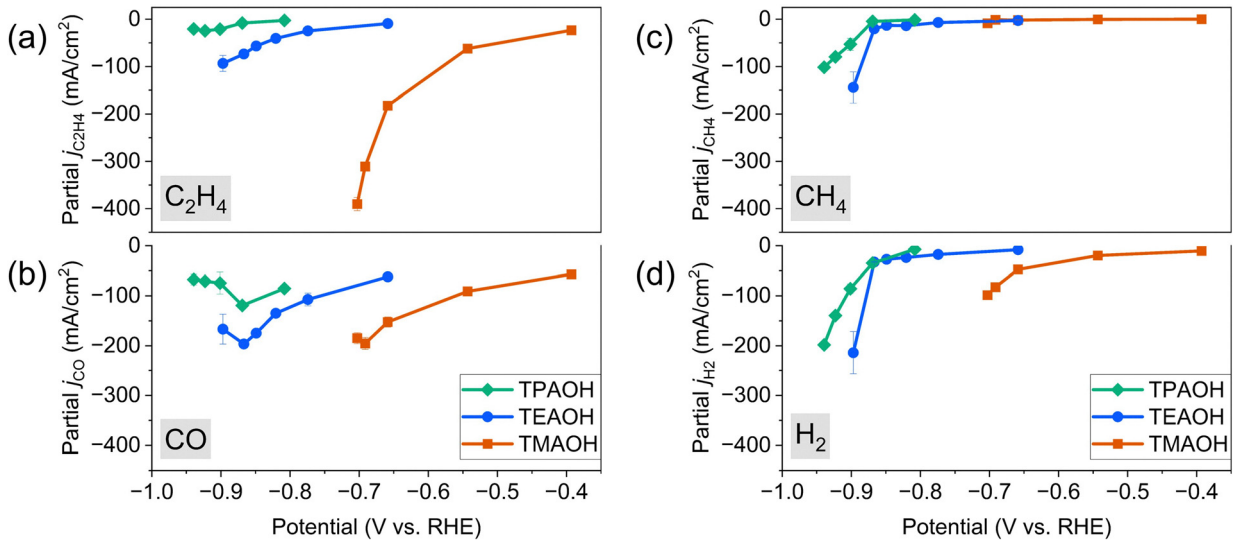

Fig. 2 Potential dependence of partial current density for (a) C_2H_4, (b) CO, (c) CH_4, and (d) H_2 in 1.0 M tetraalkylammonium hydroxide solutions.

methane formation showed less cation dependence compared with CO and ethylene formation, increasing notably at potentials more negative than −0.85 V *vs.* RHE.

In previous studies on the effect of alkali cations in the CO_2RR, the cation species have been reported to play an essential role in coordinating intermediates[19–21] or forming the electric field.[23–27] However, for tetraalkylammonium cations, the coordination effect is considered negligible because of their low Lewis acidity.[46] Thus, under the assumption that the formation of the electric field depends on the tetraalkylammonium cations, which results in variations in C_{2+} formation activity, we conducted numerical simulations to verify the electric field effect of tetraalkylammonium cations.

We calculated the local concentration of cations and the electric field strength within the Stern layer using the generalized modified Poisson–Nernst–Planck (GMPNP) model, solved with finite element methods[26,45,47–49] (see ESI† for details). We used different radius values in eqn (S1) (ESI†) for each cation species.[50] The cation density in the outer Helmholtz layer (OHP) decreased with increasing radius. Cations with a smaller radius can accumulate more densely on the electrode surface, resulting in a higher local concentration on the surface. For example, at −1.1 V *vs.* the point of zero charge (pzc), the concentration of TMA cations at the OHP was 4.2 M, whereas it decreased to 3.2 M for TEA, 2.3 M for TPA, and 1.7 M for TBA (Fig. 3a). Smaller cations create a potential distribution in

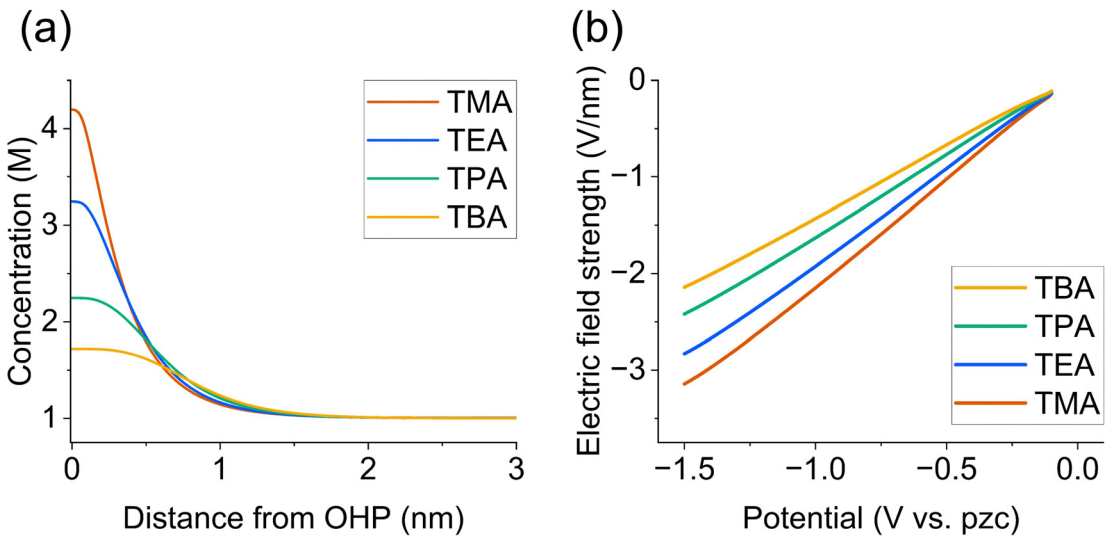

Fig. 3 (a) Local concentration of cation species near OHP, as calculated using GMPNP simulations. The concentration at an electrode potential of −1.1 V *vs.* pzc is shown as a representative example. (b) Electric field strength in Stern layer as function of electrode potential in 1.0 M tetraalkylammonium hydroxide solutions. The thickness of the Stern layer was assumed to be the radius of the cation. The electric field strength was determined on the basis of the potential distribution calculated using the Poisson equation.

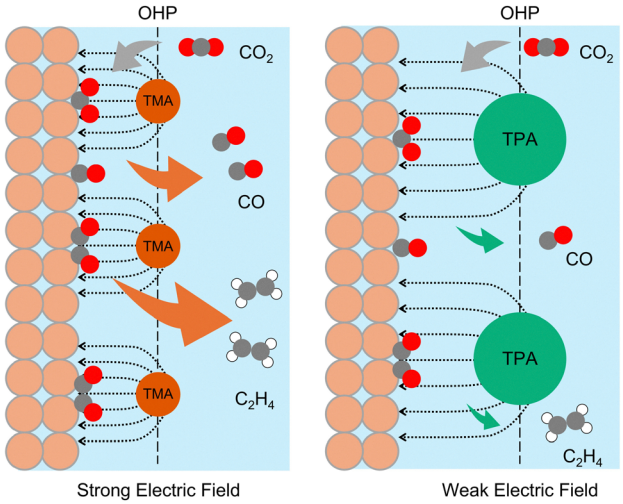

Fig. 4 Schematic of effect of different tetraalkylammonium cations on CO_2RR.

which the applied potential is more effectively pushed into the EDL (Fig. S13, ESI†). Because the potential profile and the thickness of the Stern layer are dependent on the cations, the electric field strength in the Stern layer becomes stronger as the radius of the cations decreases, even under the same applied potential conditions (Fig. 3b). At −1.1 V *vs.* pzc, the electric field values in 1.0 M TMA and TPA were −2.4 V nm^{-1} and −1.8 V nm^{-1}, respectively.

Previous studies have suggested that the electric field strength within the Stern layer affects the stability of reaction intermediates. In particular, the binding energy of reaction intermediates with dipole moments is modulated by an electric field. Reaction intermediates such as $*CO_2$ and *OCCO,[19,21,51,52] which are regarded as key species in the formation of CO and ethylene, respectively, exhibit relatively large dipole moments.[23,53] In addition, Resasco *et al.* have shown that these intermediates become more stable in the presence of strong electric fields.[23] A smaller cation, such as TMA, can enhance CO and ethylene formation by generating a stronger electric field within the Stern layer. The variation in CO_2RR activity observed with different tetraalkylammonium cations is thus likely driven by cation-size-induced changes in the electric field strength (Fig. 4). Meanwhile, methane formation is generally considered to involve the hydrogenation of *CO, forming *CHO or *COH as a key step.[54–59] Intermediates such as *COH and *CHO have been reported to have small dipole moments,[23,53] implying that the electric-field stabilization effect is considerably weaker than that for $*CO_2$ or *OCCO intermediates. In addition, the tendency for methane production at more negative potentials is consistent with earlier findings related to methane generation by Cu catalysts used in conjunction with alkali cations.[8,60–62] Therefore, methane formation is less susceptible to the electric field effects induced by different cation species and is primarily promoted in regions with large overpotentials. Namely, the electric field predominantly influences the formation of C_{2+} products and CO, thereby altering the overall selectivity of CO_2RR.

We demonstrated that C_{2+} production proceeds even when organic cations alone are used as electrolytes and that the use of smaller tetraalkylammonium cations, in particular, facilitates ethylene formation. These findings suggest that, even in electrolysis systems such as a pure-water-fed MEA in which organic ionomers serve as the sole cationic species (*i.e.*, without the use of alkali cations), the ionomer would substantially affect the rate of product formation. Although smaller cationic groups in an ionomer are considered beneficial for creating a strong electric field within the EDL, the charge density at the electrode surface is not only determined by the cation group size but also by the chemical structure of the ionomer itself. Several reports have documented C_{2+} production using ionomers in pure-water-fed MEA system.[38,41,42] However, most of these studies have focused primarily on developing electrolysis systems or optimizing reaction conditions, with limited examination of how ionomers function as cationic species influencing C_{2+} formation reactions within the EDL. As our results indicate, organic cations strongly influence C_{2+} production at the microscale level of the EDL. Therefore, focusing on the molecular-level effects of organic cations is crucial for further enhancing selectivity and improving reaction rates.

3. Conclusions

In summary, we conducted the CO_2RR in aqueous solutions containing tetraalkylammonium cations to investigate the effect of cation species on product formation. We confirmed that ethylene and CO production rates increased when smaller cations were used. Specifically, the partial current density for ethylene reached 390 mA cm^{-2} with the tetramethylammonium cation, whereas it was substantially lower for tetraethylammonium and tetrapropylammonium cations (93.4 mA cm^{-2} and 24.6 mA cm^{-2}, respectively). By contrast, methane formation exhibited a minimal dependence on the cation species. Numerical simulations revealed that tetraalkylammonium cations influence the electric field strength within the EDL, with smaller cations generating a stronger field because of their smaller radii. This enhanced electric field is considered to stabilize reaction intermediates. The proposed mechanism for CO and ethylene formation in the presence of tetraalkylammonium cations highlights that the formation rates of these products increase with decreasing cation size because the higher concentration of smaller cations at the OHP and the thinner Stern layer intensify the electric field inside the EDL, thereby stabilizing key intermediates. These findings underscore the critical importance of cation design in optimizing CO_2 electrolysis and provide a foundation for the future exploration of highly selective and stable electrolysis systems. Even in alkali-cation-free systems such as pure-water-fed MEAs, the effect of organic cations is considered to play a critical role.

Conflicts of interest

There are no conflicts to declare.

Data availability

The data supporting this article have been included as part of the ESI.†

Acknowledgements

This work was supported by JST-CREST (grant JPMJCR24S6), Japan. This work was also supported by a JSPS KAKENHI Program (grant 23H02063) and JST SPRING (grant JPMJSP 2138). Synchrotron radiation experiments were performed using the BL01B1 beamline of SPring-8 with approval of the Japan Synchrotron Radiation Research Institute (Proposals 2023A1690 and 2024B2030).

References

1 K. Kamiya, K. Fujii, M. Sugiyama and S. Nakanishi, *Chem. Lett.*, 2021, **50**, 166–179.
2 P. De Luna, C. Hahn, D. Higgins, S. A. Jaffer, T. F. Jaramillo and E. H. Sargent, *Science*, 2019, **364**, eaav3506.
3 G. A. Olah, G. K. S. Prakash and A. Goeppert, *J. Am. Chem. Soc.*, 2011, **133**, 12881–12898.
4 S. Nitopi, E. Bertheussen, S. B. Scott, X. Liu, A. K. Engstfeld, S. Horch, B. Seger, I. E. L. Stephens, K. Chan, C. Hahn, J. K. Nørskov, T. F. Jaramillo and I. Chorkendorff, *Chem. Rev.*, 2019, **119**, 7610–7672.
5 Y. Y. Birdja, E. Pérez-Gallent, M. C. Figueiredo, A. J. Göttle, F. Calle-Vallejo and M. T. M. Koper, *Nat. Energy*, 2019, **4**, 732–745.
6 W. Zhang, Y. Hu, L. Ma, G. Zhu, Y. Wang, X. Xue, R. Chen, S. Yang and Z. Jin, *Adv. Sci.*, 2018, **5**, 1700275.
7 Y. Hori, K. Kikuchi, A. Murata and S. Suzuki, *Chem. Lett.*, 1986, 897–898.
8 Y. Hori, A. Murata and R. Takahashi, *J. Chem. Soc. Lond. Faraday Trans. 1*, 1989, **85**, 2309–2326.
9 Y. Hori, H. Wakebe, T. Tsukamoto and O. Koga, *Electrochim. Acta*, 1994, **39**, 1833–1839.
10 A. Bagger, W. Ju, A. S. Varela, P. Strasser and J. Rossmeisl, *Chem. Phys. Chem.*, 2017, **18**, 3266–3273.
11 C.-T. Dinh, T. Burdyny, M. G. Kibria, A. Seifitokaldani, C. M. Gabardo, F. P. García de Arquer, A. Kiani, J. P. Edwards, P. De Luna, O. S. Bushuyev, C. Zou, R. Quintero-Bermudez, Y. Pang, D. Sinton and E. H. Sargent, *Science*, 2018, **360**, 783–787.
12 Y. Wu, K. Iwase, T. Harada, S. Nakanishi and K. Kamiya, *ACS Appl. Nano Mater.*, 2021, **4**, 4994–5003.
13 A. Inoue, T. Harada, S. Nakanishi and K. Kamiya, *EES. Catal.*, 2023, **1**, 9–16.
14 R. Kurihara, K. Nagita, K. Ohashi, Y. Mukouyama, T. Harada, S. Nakanishi and K. Kamiya, *Adv. Mater. Interfaces*, 2024, **11**, 2300731.
15 L. Fan, C. Xia, F. Yang, J. Wang, H. Wang and Y. Lu, *Sci. Adv.*, 2020, **6**, eaay3111.
16 C. P. O'Brien, R. K. Miao, A. Shayesteh Zeraati, G. Lee, E. H. Sargent and D. Sinton, *Chem. Rev.*, 2024, **124**, 3648–3693.
17 E. W. Lees, B. A. W. Mowbray, F. G. L. Parlane and C. P. Berlinguette, *Nat. Rev. Mater.*, 2021, **7**, 55–64.
18 R. Kortlever, J. Shen, K. J. P. Schouten, F. Calle-Vallejo and M. T. M. Koper, *J. Phys. Chem. Lett.*, 2015, **6**, 4073–4082.
19 M. C. O. Monteiro, F. Dattila, B. Hagedoorn, R. García-Muelas, N. López and M. T. M. Koper, *Nat. Catal.*, 2021, **4**, 654–662.
20 H. Liu, J. Liu and B. Yang, *ACS Catal.*, 2021, **11**, 12336–12343.
21 S.-J. Shin, H. Choi, S. Ringe, D. H. Won, H.-S. Oh, D. H. Kim, T. Lee, D.-H. Nam, H. Kim and C. H. Choi, *Nat. Commun.*, 2022, **13**, 5482.
22 X. Qin, T. Vegge and H. A. Hansen, *J. Am. Chem. Soc.*, 2023, **145**, 1897–1905.
23 J. Resasco, L. D. Chen, E. Clark, C. Tsai, C. Hahn, T. F. Jaramillo, K. Chan and A. T. Bell, *J. Am. Chem. Soc.*, 2017, **139**, 11277–11287.
24 S. Ringe, E. L. Clark, J. Resasco, A. Walton, B. Seger, A. T. Bell and K. Chan, *Energy Environ. Sci.*, 2019, **12**, 3001–3014.
25 L. D. Chen, M. Urushihara, K. Chan and J. K. Nørskov, *ACS Catal.*, 2016, **6**, 7133–7139.
26 H.-G. Qin, F.-Z. Li, Y.-F. Du, L.-F. Yang, H. Wang, Y.-Y. Bai, M. Lin and J. Gu, *ACS Catal.*, 2023, **13**, 916–926.
27 J. Gu, S. Liu, W. Ni, W. Ren, S. Haussener and X. Hu, *Nat. Catal.*, 2022, **5**, 268–276.
28 S. Kato, S. Ito, S. Nakahata, R. Kurihara, T. Harada, S. Nakanishi and K. Kamiya, *ChemSusChem*, 2024, **17**, e202401013.
29 S. Garg, Q. Xu, A. B. Moss, M. Mirolo, W. Deng, I. Chorkendorff, J. Drnec and B. Seger, *Energy Environ. Sci.*, 2023, **16**, 1631–1643.
30 M. Sassenburg, M. Kelly, S. Subramanian, W. A. Smith and T. Burdyny, *ACS Energy Lett.*, 2023, **8**, 321–331.
31 Q. Bai, L. Xiong, Y. Zhang, M. Ma, Z. Jiao, F. Lyu, Z. Deng and Y. Peng, *EES. Catal.*, 2024, **2**, 1228–1237.
32 S. Weng, W. L. Toh and Y. Surendranath, *J. Am. Chem. Soc.*, 2023, **145**, 16787–16795.
33 H. Jang, A. M. Gardner, L. J. Walters, A. R. Neale, L. J. Hardwick and A. J. Cowan, *ACS Electrochem.*, 2025, **1**, 20–24.
34 S. Banerjee, Z.-Q. Zhang, A. S. Hall and V. S. Thoi, *ACS Catal.*, 2020, **10**, 9907–9914.
35 Y. Zhong, Y. Xu, J. Ma, C. Wang, S. Sheng, C. Cheng, M. Li, L. Han, L. Zhou, Z. Cai, Y. Kuang, Z. Liang and X. Sun, *Angew. Chem., Int. Ed.*, 2020, **59**, 19095–19101.
36 J. Wang, T. Cheng, A. Q. Fenwick, T. N. Baroud, A. Rosas-Hernández, J. H. Ko, Q. Gan, W. A. Goddard III and R. H. Grubbs, *J. Am. Chem. Soc.*, 2021, **143**, 2857–2865.
37 Y. I. Song, B. Yoon, C. Lee, D. Kim, M. H. Han, H. Han, W. H. Lee, D. H. Won, J. K. Kim, H. S. Jeon and J. H. Koh, *Adv. Sci.*, 2024, **11**, e2406281.
38 L. Xue, Z. Gao, T. Ning, W. Li, J. Li, J. Yin, L. Xiao, G. Wang and L. Zhuang, *Angew. Chem., Int. Ed.*, 2023, **62**, e202309519.
39 Z. Gao, L. Xue, X. Hu, J. Yin, L. Xiao, G. Wang, J. Lu and L. Zhuang, *Electrochim. Acta*, 2023, **458**, 142509.

40 J. Y. Zhao, Y. Liu, W. Li, C. F. Wen, H. Q. Fu, H. Y. Yuan, P. F. Liu and H. G. Yang, *Chem. Catal.*, 2023, **3**, 100471.
41 W. Li, Z. Yin, Z. Gao, G. Wang, Z. Li, F. Wei, X. Wei, H. Peng, X. Hu, L. Xiao, J. Lu and L. Zhuang, *Nat. Energy*, 2022, **7**, 835–843.
42 X. She, L. Zhai, Y. Wang, P. Xiong, M. M.-J. Li, T.-S. Wu, M. C. Wong, X. Guo, Z. Xu, H. Li, H. Xu, Y. Zhu, S. C. E. Tsang and S. P. Lau, *Nat. Energy*, 2024, **9**, 81–91.
43 K. Liu, W. A. Smith and T. Burdyny, *ACS Energy Lett.*, 2019, **4**, 639–643.
44 A. R. Heenan, J. Hamonnet and A. T. Marshall, *ACS Energy Lett.*, 2022, **7**, 2357–2361.
45 M. Fan, J. E. Huang, R. K. Miao, Y. Mao, P. Ou, F. Li, X.-Y. Li, Y. Cao, Z. Zhang, J. Zhang, Y. Yan, A. Ozden, W. Ni, Y. Wang, Y. Zhao, Z. Chen, B. Khatir, C. P. O'Brien, Y. Xu, Y. C. Xiao, G. I. N. Waterhouse, K. Golovin, Z. Wang, E. H. Sargent and D. Sinton, *Nat. Catal.*, 2023, **6**, 763–772.
46 K. Ueno, H. Tokuda and M. Watanabe, *Phys. Chem. Chem. Phys.*, 2010, **12**, 1649–1658.
47 D. Bohra, J. H. Chaudhry, T. Burdyny, E. A. Pidko and W. A. Smith, *Energy Environ. Sci.*, 2019, **12**, 3380–3389.
48 M. S. Kilic, M. Z. Bazant and A. Ajdari, *Phys. Rev. E: Stat., Nonlinear, Soft Matter Phys.*, 2007, **75**, 021503.
49 E. F. Johnson, E. Boutin and S. Haussener, *J. Phys. Chem. C*, 2023, **127**, 18784–18790.
50 E. R. Nightingale Jr, *J. Phys. Chem.*, 1959, **63**, 1381–1387.
51 J. H. Montoya, C. Shi, K. Chan and J. K. Nørskov, *J. Phys. Chem. Lett.*, 2015, **6**, 2032–2037.
52 W. Deng, P. Zhang, Y. Qiao, G. Kastlunger, N. Govindarajan, A. Xu, I. Chorkendorff, B. Seger and J. Gong, *Nat. Commun.*, 2024, **15**, 892.
53 H. Peng, M. T. Tang, X. Liu, P. Schlexer Lamoureux, M. Bajdich and F. Abild-Pedersen, *Energy Environ. Sci.*, 2021, **14**, 473–482.
54 X. Nie, W. Luo, M. J. Janik and A. Asthagiri, *J. Catal.*, 2014, **312**, 108–122.
55 W. Luo, X. Nie, M. J. Janik and A. Asthagiri, *ACS Catal.*, 2016, **6**, 219–229.
56 X. Liu, J. Xiao, H. Peng, X. Hong, K. Chan and J. K. Nørskov, *Nat. Commun.*, 2017, **8**, 15438.
57 X. Liu, P. Schlexer, J. Xiao, Y. Ji, L. Wang, R. B. Sandberg, M. Tang, K. S. Brown, H. Peng, S. Ringe, C. Hahn, T. F. Jaramillo, J. K. Nørskov and K. Chan, *Nat. Commun.*, 2019, **10**, 32.
58 M. T. Tang, H. Peng, P. S. Lamoureux, M. Bajdich and F. Abild-Pedersen, *Appl. Catal., B*, 2020, **279**, 119384.
59 J. Li, X. Chang, H. Zhang, A. S. Malkani, M.-J. Cheng, B. Xu and Q. Lu, *Nat. Commun.*, 2021, **12**, 3264.
60 K. J. P. Schouten, Y. Kwon, C. J. M. van der Ham, Z. Qin and M. T. M. Koper, *Chem. Sci.*, 2011, **2**, 1902–1909.
61 K. P. Kuhl, E. R. Cave, D. N. Abram and T. F. Jaramillo, *Energy Environ. Sci.*, 2012, **5**, 7050–7059.
62 Y. Huang, A. D. Handoko, P. Hirunsit and B. S. Yeo, *ACS Catal.*, 2017, **7**, 1749–1756.